

REDISCUSSION OF ECLIPSING BINARIES. PAPER 20:  
HO TEL CHECKOUT

By John Southworth

*Astrophysics Group, Keele University*

We present a detailed analysis of the detached eclipsing binary system HO Telescopii, which contains two A-type stars in a circular orbit of period 1.613 d. We use light-curves from the *Transiting Exoplanet Survey Satellite (TESS)*, which observed HO Tel in three sectors, to determine its photometric properties and a precise orbital ephemeris. We augment these results with radial-velocity measurements from Sürgit *et al.*<sup>1</sup> to determine the masses and radii of the component stars:

$$M_A = 1.906 \pm 0.031 M_\odot, M_B = 1.751 \pm 0.034 M_\odot, \\ R_A = 2.296 \pm 0.027 R_\odot \text{ and } R_B = 2.074 \pm 0.028 R_\odot.$$

Combined with temperature measurements from Sürgit *et al.*<sup>1</sup> and optical-infrared apparent magnitudes from the literature, we find a distance to the system of  $280.8 \pm 4.6$  pc which agrees well with the distance from the *Gaia* DR3 parallax measurement. Theoretical predictions do not quite match the properties of the system, and there are small discrepancies in measurements of the spectroscopic orbits of the stars. Future observations from *Gaia* will allow further investigation of these issues.

### Introduction

In the current series of papers we are performing detailed photometric analyses of a set of known detached eclipsing binaries (dEBs) for which space-based light-curves are available but have not been studied previously, and which have published spectroscopic mass measurements. The aim is to increase the number of stars with precisely-measured masses and radii against which theoretical stellar models can be compared<sup>2-5</sup>. A detailed exposition of these goals can be found in the first paper of the series (ref. 6) and a review of the impact of space telescopes in this scientific area can be found in ref. 7.

In this work we investigate the dEB HO Telescopii (Table I), which contains two late-A type stars in a circular orbit of period 1.613 d. Its variability was discovered by Strohmeier *et al.*<sup>8</sup> under the designation BV 590, and its correct orbital period was determined by Spoelstra & van Houten<sup>9</sup>. Subsequent work on this object has been nicely summarized by Sürgit *et al.*<sup>1</sup> (hereafter S17). These authors presented radial-velocity (RV) measurements from medium-resolution spectra obtained with the *SpUpNIC* spectrograph<sup>10</sup> on the 74-inch *Radcliffe* telescope at the South African Astronomical Observatory. S17 combined these RVs with five-colour (Walraven<sup>11</sup> *VBLUW*) light-curves from Spoelstra & van Houten<sup>9</sup> and the light-curve from the All-Sky Automated Survey (ASAS<sup>12</sup>) to measure the properties of the system. Below we use the same RVs and new space-based data to refine the measurements of the system properties.

TABLE I

Basic information on HO Telescopii. The BV magnitudes are each the mean of 110 individual measurements<sup>13</sup>.

Property	Value	Reference
Right ascension (J2000)	19 <sup>h</sup> 51 <sup>m</sup> 58 <sup>s</sup> .93	14
Declination (J2000)	-46°51'42".4	14
Henry Draper designation	HD 187418	15
Gaia DR3 designation	6671501451113955072	14
Gaia DR3 parallax	3.5186 ± 0.0314 mas	14
TESS Input Catalog designation	TIC 80064289	16
B magnitude	8.59 ± 0.03	13
V magnitude	8.31 ± 0.01	13
J magnitude	7.814 ± 0.027	17
H magnitude	7.776 ± 0.029	17
K <sub>s</sub> magnitude	7.730 ± 0.018	17
Spectral type	A7V + A8V	1

### Photometric observations

HO Tel has been observed in three sectors by the *Transiting Exoplanet Survey Satellite* (TESS<sup>18</sup>): sector 13 (2019 July) where the observations were summed into cadences of 1800-s duration; sector 27 with a cadence of 600 s; and sector-67 with a cadence of 200 s. We downloaded the data for all sectors from the NASA Mikulski Archive for Space Telescopes (MAST<sup>\*</sup>) using the LIGHTKURVE package<sup>19</sup>. However, we restricted our analysis below to the data from sector 67 due to its better sampling rate. We adopted the simple aperture photometry (SAP) data from the TESS-SPOC data reduction<sup>20</sup> with a quality flag of “hard”. These were normalized using LIGHTKURVE and converted to differential magnitudes.

The light-curve from sector 67 is shown in Fig. 1. Four regions of data (one of which is outside the figure) were removed from our analysis due to incomplete coverage of eclipses or decreased photometric precision due to scattered light from Earth: we kept 8006 of the original 9332 data points. The primary eclipse is clearly deeper than the secondary. We label the star eclipsed during primary minimum star A and its companion star B.

We queried the Gaia DR3 database<sup>†</sup> and found a total of 75 objects within 2 arcmin of the sky position of HO Tel. Of these, the brightest is fainter than our target by 4.5 mag in the  $G_{\text{RP}}$  band, and the remainder are fainter by at least 5.7 mag in that band. This suggests that the TESS light-curve of HO Tel will be contaminated by light from nearby stars at the level of only a few percent.

### Preliminary light-curve analysis

The components of HO Tel are close and significantly distorted from sphericity. However, the number of data points is large enough to make an analysis with a code implementing Roche geometry slow. We have therefore undertaken a preliminary analysis with a simpler code to determine the orbital

\* <https://mast.stsci.edu/portal/Mashup/Clients/Mast/Portal.html>

† <https://vizier.cds.unistra.fr/viz-bin/VizieR-3?-source=1/355/gaiadr3>

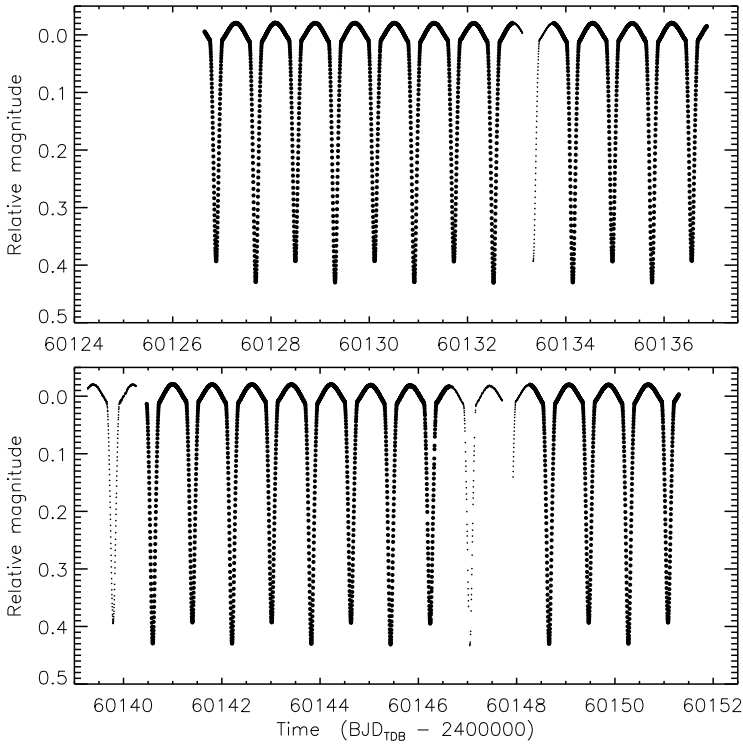


FIG. 1

*TESS* short-cadence SAP photometry of HO Tel from sector 67. The flux measurements have been converted to magnitude units then rectified to zero magnitude by subtraction of the median. The two panels show half the sector each. Larger points show the data retained for analysis and smaller points the data rejected due to offsets or increased scatter.

ephemeris and enable the construction of a phase-binned light-curve.

We modelled the *TESS* sector-67 light-curve using version 43 of the JKTEBOP\* code<sup>21,22</sup> using a suitable set of adjustable parameters (see previous papers in this series). Once a good fit was achieved, the *TESS* observations were converted to orbital phase and binned into 1000 points equally-spaced in phase. This phase-binned light-curve retains practically all the information of the original data whilst containing a factor of eight fewer data points.

We refined the orbital ephemeris of HO Tel by adding new and published times of mid-eclipse to our JKTEBOP fit. We included the four times from Sestero & Candellero<sup>23</sup>, and the four times from Spoelstra & Van Houten<sup>9</sup>. Uncertainties were not quoted for those measurements so we adopted an error bar of  $\pm 0.003$  d for each. We also measured three additional times of primary eclipse by fitting the *TESS* sectors individually. The precision of these eclipse times is extraordinary (0.3 to 0.9 s) but appears to be justified. The early times were converted to the  $\text{BJD}_{\text{TDB}}$  time-scale<sup>24</sup> to match the *TESS* data.

We also tried to include the timing from table 2 of S17 but found it to deviate from a linear ephemeris by +30.8 min; conversion from the original HJD

\*<http://www.astro.keele.ac.uk/jkt/codes/jktebop.html>

(presumed UTC) to the  $\text{BJD}_{\text{TDB}}$  time-scale used in the current paper would add a further 65 s to this discrepancy. The issue probably arises from the use of an old time of conjunction combined with a fixed period, which is not a problem for fitting the RV curve but does make the timing unsuitable for determining the orbital period. We therefore excluded it from our analysis.

The ephemeris was obtained as part of our JKTEBOP solution in the preceding section and is

$$\text{Min I} = \text{BJD}_{\text{TDB}} 2460135.755972(3) + E \times 1.613103937(8), \quad (1)$$

where  $E$  is the cycle number and the bracketed quantities represent the uncertainty in the final digit of the preceding number. The individual eclipse times and their residuals *versus* this linear ephemeris are given in Table II. We see no evidence in these data for a deviation from a constant orbital period.

TABLE II

*Times of published mid-eclipse for HO Tel and their residuals versus the best fit reported in the current work. Each residual is given as a fraction of the uncertainty. The asterisk indicates the time not included in the final best fit, to avoid double-use of data. The orbital cycle is an integer for primary eclipses and a half-integer for secondary eclipses.*

Orbital cycle	Eclipse time ( $\text{BJD}_{\text{TDB}}$ )	Uncertainty (d)	Best fit ( $\text{BJD}_{\text{TDB}}$ )	Residual ( $\sigma$ )	Source
-13113.5	2438982.31756	0.003	2438982.31750	1.12	23
-13113	2438986.34984	0.003	2438986.35026	0.28	23
-13108.5	2438990.38244	0.003	2438990.38302	0.34	23
-13087.5	2439024.25888	0.003	2439024.25821	-0.08	23
-11072.5	2442274.65961	0.003	2442274.66264	1.18	9
-11072	2442275.47641	0.003	2442275.46919	-2.24	9
-10886.5	2442574.70254	0.003	2442574.69997	-0.68	9
-10649	2442957.81126	0.003	2442957.81216	0.48	9
-909	2458669.444500	0.000010	2458669.444494	-0.61	This work
-673	2459050.137019	0.000007	2459050.137023	0.57	This work
0*	2460135.755971	0.000003			This work

### *Analysis with the Wilson-Devinney code*

The main analysis of the light-curve was performed using the Wilson-Devinney (WD) code<sup>25,26</sup>, which implements Roche geometry to represent accurately the shapes of distorted stars. We used the 2004 version of the code (WD2004), driven by the JKTWD wrapper<sup>27</sup>, to fit the phase-binned light-curve from the previous section. Below we describe the adopted solution of the light-curve, followed by the error analysis. The parameters in the WD2004 code are described in its accompanying user manual (ref. 28).

For our adopted solution we fitted for the potentials and light contributions of the two stars, the orbital inclination, and one limb-darkening coefficient per star. Limb darkening was implemented using the logarithmic law with the linear coefficients fitted and the nonlinear coefficients fixed at theoretical values from Van Hamme<sup>29</sup>. We also had to fit for the albedo of both stars and for third light to obtain a good fit to the data. We used mode 0, where the effective temperatures ( $T_{\text{eff}}$ s) and light contributions are decoupled, and fixed the  $T_{\text{eff}}$ s to values from S17. We adopted a circular orbit, the mass ratio from S17, the simple model of reflection, synchronous rotation, gravity-darkening exponents of 1.0 (suitable for radiative atmospheres), the maximum possible numerical precision of  $\text{N1} = \text{N2} = 60$ , and the Johnson  $R$  passband as representative of the *TESS* passband for stars like those in HO Tel. With this approach we obtained a good fit to the data (Fig. 2) which has residuals that are small but do show a trend with orbital

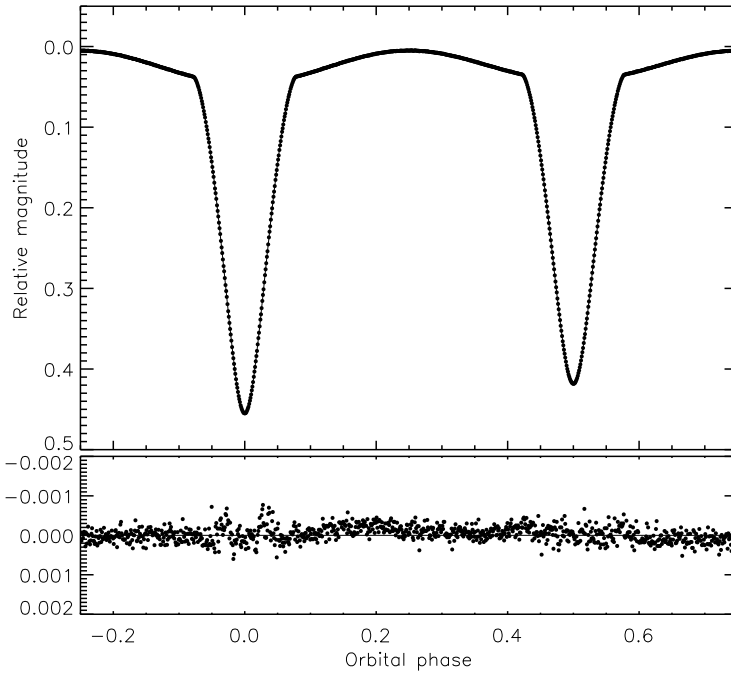


FIG. 2

Best fit to the binned light-curve of HO Tel using wd2004. The phase-binned data are shown using open circles and the best fit with a continuous line. The residuals are shown on an enlarged scale in the lower panel.

phase. The parameters of this fit are given in Table III.

The error bars returned by wd2004 account for the scatter of the data but not for the many choices made during the modelling process, so are far too small. To determine realistic error bars we performed a large number of alternative modelling runs whilst varying the input physics and treatment of the data. These differences were: using mode 2 and fitting for  $T_{\text{eff}}$  instead of the light contribution of star B; changing the spectroscopic mass ratio by its uncertainty; changing the rotation rates by  $\pm 0.1$ ; changing the gravity-darkening exponents by  $\pm 0.1$ ; fitting for a phase shift; fixing the limb-darkening coefficients at the theoretically-predicted values; using the square-root limb-darkening law; using the Johnson  $I$  passband instead of  $R$ ; changing the numerical precision values ( $N1$  and  $N2$ ) to 59, 58, 57, or 56; using the detailed reflection-effect option; using two instead of one reflection with the detailed reflection treatment; using a light-curve phase-binned into 500 instead of 1000 points; and removing the polynomials from the JKTEBOP fit before binning. This process is basically the same as has been used for numerous systems in the past<sup>30–33</sup>.

The result of this process was a large set of different parameter values. The differences for each parameter *versus* the adopted solution were added in quadrature to obtain the final uncertainty for that parameter. These error bars

TABLE III

Summary of the parameters for the WD2004 solution of the TESS light-curve of HO Tel. Uncertainties are only quoted when they have been assessed by comparison between a full set of alternative solutions.

Parameter	Star A	Star B
<i>Control parameters:</i>		
WD2004 operation mode		0
Treatment of reflection		1
Number of reflections		1
Limb-darkening law		2 (logarithmic)
Numerical grid size normal		60
Numerical grid size coarse		60
<i>Fixed parameters:</i>		
Phase shift		0.0
Mass ratio		0.921
Rotation rates	1.0	1.0
Gravity darkening	1.0	1.0
$T_{\text{eff}}$ values (K)	7872	7627
Bolometric linear LD coefficient	0.6720	0.6799
Bolometric logarithmic LD coefficient	0.1991	0.2043
Passband logarithmic LD coefficient	0.2454	0.2430
<i>Fitted parameters:</i>		
Bolometric albedos	$1.20 \pm 0.40$	$1.00 \pm 0.24$
Potential	$4.848 \pm 0.048$	$5.036 \pm 0.051$
Orbital inclination ( $^{\circ}$ )		$81.041 \pm 0.067$
Light contributions	$6.92 \pm 0.19$	$5.19 \pm 0.18$
Passband linear LD coefficient	$0.579 \pm 0.017$	$0.550 \pm 0.017$
Third light		$0.016 \pm 0.013$
<i>Derived parameters:</i>		
Fractional radii	$0.2575 \pm 0.0026$	$0.2325 \pm 0.0029$
Light ratio		$0.754 \pm 0.036$

TABLE IV

Changes in the measured fractional radii of the stars due to differing model choices. Each is expressed as the percentage change versus the value of the parameter.

Model choice	Effect (%)	
	$r_A$	$r_B$
Changing mass ratio	0.38	-0.56
Changing rotation rates by $\pm 0.1$	0.28	-0.21
Changing gravity darkening by $\pm 0.1$	0.03	-0.02
Fitting for phase shift	0.00	0.00
Fixing limb-darkening coefficients	0.34	-0.18
Using the square-root limb-darkening law	-0.01	-0.04
Using the Johnson <i>I</i> -band	0.10	-0.16
Setting the numerical precision to $N1=N2=58$	0.82	-1.02
Using the detailed treatment of reflection	0.01	0.00
Detailed treatment of reflection with two reflections	0.01	-0.00
Modelling a light-curve of 500 phase-binned data points	0.09	-0.13
Removing the polynomial normalization	0.05	-0.19

are reported in Table III. The albedos and third-light values are quite uncertain: their error bars are dominated by the variation obtained when using the Johnson *I* band instead of the *R* band.

The fractional radii of the stars are determined to 1.0% and 1.3% precision, respectively, but the main source of uncertainty is unexpected. To illustrate

this we give in Table IV the individual contributions to the uncertainties in the fractional radii which arise from the various model choices listed above. The largest effect is due to the choice of numerical precision, which sets a limit on how well the fractional radii ( $r_A$  and  $r_B$ ) can be measured. We have previously seen this effect in our analysis of the eclipsing system KIC 4851217 (Jennings *et al.*, submitted) so the current result is not an isolated incident. It is likely that more sophisticated modelling codes<sup>34</sup> will suffer less from this effect and thus allow an increase in the precision achievable in the determination of the properties of distorted stars in eclipsing binary systems.

### Radial-velocity analysis

S17 obtained 45 medium-resolution spectra, from each of which they measured RVs for both stars using cross-correlation. These were included in their analysis with the WD code and the resulting parameters were given with 90% confidence intervals. As we universally use standard errors we have reanalysed the RVs to determine our own spectroscopic orbital parameters.

The RVs were obtained from table 1 in S17 and modelled using the JKTEBOP code, with the orbital ephemeris from above but with no other constraints from the *TESS* light-curve. The quoted error bars were scaled so the fit to the RVs of each star had a reduced  $\chi^2$  value of unity. We fitted for the velocity amplitudes of the stars and the systemic velocity of the system, obtaining  $K_A = 132.3 \pm 1.2$  km s<sup>-1</sup>,  $K_B = 144.0 \pm 1.0$  km s<sup>-1</sup>, and  $V_\gamma = -5.5 \pm 0.6$  km s<sup>-1</sup>, respectively. The error bars for these quantities were obtained using Monte Carlo simulations<sup>35</sup>. If the systemic velocities of the two stars are fitted separately there is a difference of 3.9 km s<sup>-1</sup> between the stars, and the  $K_A$  and  $K_B$  change by -0.4 km s<sup>-1</sup>.

The best fit to the RVs is shown in Fig. 3. It can be seen that there are three spectra which give large residuals, around phases 0.13 and 0.59. If these are rejected the measured properties become  $K_A = 133.9 \pm 1.2$  km s<sup>-1</sup>,  $K_B = 145.5 \pm 0.8$  km s<sup>-1</sup>, and  $V_\gamma = -4.4 \pm 0.5$  km s<sup>-1</sup>. We chose not to adopt these values, because there were no clear reasons to reject those data, but report them for completeness.

The spectroscopic orbital parameters given by S17 agree with our own results, and are  $K_A = 131.5 \pm 1.2$  km s<sup>-1</sup>,  $K_B = 142.8 \pm 1.2$  km s<sup>-1</sup>, and  $V_\gamma = -5.9 \pm 0.7$  km s<sup>-1</sup>. A cross-check of these numbers is also available using the *Gaia*<sup>36</sup> DR3<sup>37</sup> tbsob2 catalogue<sup>38</sup>, which includes the parameters of a double-lined spectroscopic orbit for the system. Based on 12 RVs for each star the orbit is  $K_A = 136.8 \pm 1.2$  km s<sup>-1</sup>,  $K_B = 144.5 \pm 1.2$  km s<sup>-1</sup>, and  $V_\gamma = -7.5 \pm 0.6$  km s<sup>-1</sup>. The velocity amplitude of star A is somewhat higher than that found from the RVs of S17, but this cannot have been investigated further because the individual RVs from *Gaia* have not been made publicly available. A small disagreement was also found in our analysis of V570 Per<sup>39</sup>, and other issues have been noted in the literature<sup>40-42</sup>, so we look forward to the RV measurements and individual spectra becoming available in future.

### Physical properties and distance to HO Tel

The physical properties of HO Tel were determined from the results of the wd2004 code and RV analyses given above, using the JKTEBOP code<sup>44</sup> (Table V). The masses and radii of the component stars are now known to 2% or better, matching the minimum requirements for a useful comparison with theoretical models<sup>2,45</sup>. Our results agree well with those from S17, but the availability of the *TESS* data has allowed us to improve the measurement precision of the radii

\* <https://vizier.cds.unistra.fr/viz-bin/VizieR-3?-source=I/357/tbsob2>

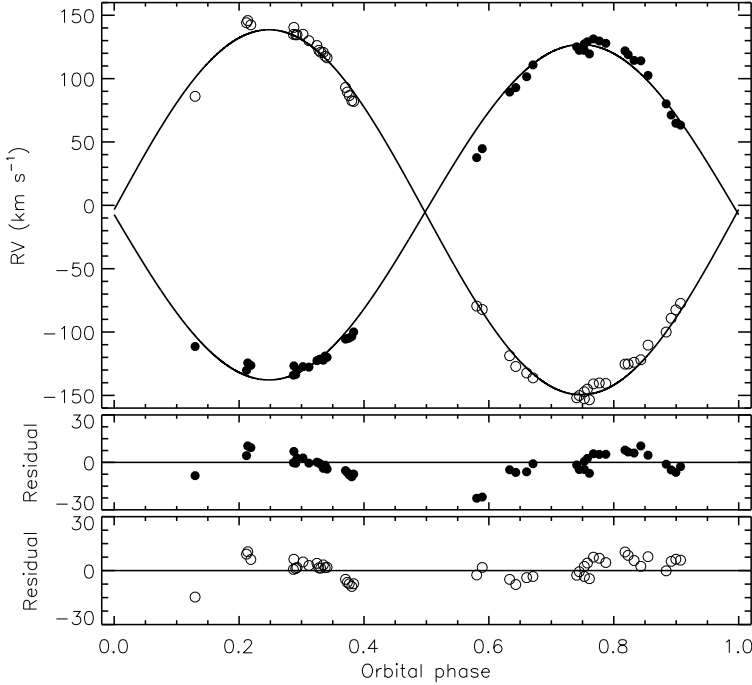


FIG. 3

RVs of HO Tel from S17 (filled circles for star A and open circles for star B), compared to the best fit from JKTEBOP (solid lines). The residuals are given in the lower panels separately for the two components.

TABLE V

Physical properties of HO Tel defined using the nominal solar units given by IAU 2015 Resolution B3 (ref. 43).

Parameter	Star A	Star B
Mass ratio $M_B/M_A$		$0.919 \pm 0.010$
Semi-major axis of relative orbit ( $R_\odot^N$ )		$8.918 \pm 0.050$
Mass ( $M_\odot^N$ )	$1.906 \pm 0.031$	$1.751 \pm 0.034$
Radius ( $R_\odot^N$ )	$2.296 \pm 0.027$	$2.074 \pm 0.028$
Surface gravity ( $\log[cgs]$ )	$3.996 \pm 0.009$	$4.048 \pm 0.012$
Density ( $\rho_\odot$ )	$0.1574 \pm 0.0048$	$0.1965 \pm 0.0075$
Synchronous rotational velocity ( $\text{km s}^{-1}$ )	$72.03 \pm 0.83$	$65.03 \pm 0.89$
Effective temperature (K)	$7872 \pm 200$	$7627 \pm 201$
Luminosity ( $\log(L/L_\odot^N)$ )	$1.261 \pm 0.045$	$1.118 \pm 0.047$
$M_{\text{bol}}$ (mag)	$1.59 \pm 0.11$	$1.95 \pm 0.12$
Interstellar reddening $E(B-V)$ (mag)		$0.04 \pm 0.02$
Distance (pc)		$280.8 \pm 4.6$

from 7% to 1%.

To determine the distance to the system we adopted the  $T_{\text{eff}}$  measurements from S17, the  $BV$  and  $\mathcal{J}HK_s$  magnitudes from Table I, the surface-brightness calibrations from Kervella *et al.*<sup>46</sup>, and the method from Southworth *et al.*<sup>44</sup>. The 2MASS  $\mathcal{J}HK_s$  magnitudes were obtained at orbital phase 0.796. A small interstellar reddening of  $E(B-V) = 0.04 \pm 0.02$  was needed to bring the

distances from the  $BV$  bands into agreement with those from the  $\mathcal{JHK}_s$  bands. The resulting distance of  $280.8 \pm 4.6$  pc agrees with the value of  $284.2 \pm 3.2$  pc from the *Gaia* DR3 parallax.

### Conclusion

The dEB HO Tel contains two A-type stars in a short-period orbit which causes them to be tidally deformed. We have determined their masses and radii using photometry from the *TESS* mission and published ground-based RVs from S17. The measurements are to 1.6% and 1.9% precision in mass, and 1.2% and 1.0% precision in radius. The mass measurements are limited by the scatter in the available RVs, and the radius measurements by the numerical precision of the modelling code used. Adding published  $T_{\text{eff}}$ s and apparent magnitudes to the analysis allowed a measurement of the distance to the system of  $281 \pm 5$  pc, in agreement with the distance from *Gaia* DR3.

We have compared the measured properties of the component stars to the predictions of the PARSEC theoretical stellar-evolutionary models<sup>47</sup>. We confirm the discrepancy found by S17 in that a good fit to both stars cannot be obtained for a single age, and that star B matches predictions for older ages ( $1030 \pm 70$  Myr) than star A ( $880 \pm 60$  Myr) for a solar metal abundance ( $Z = 0.017$ ). The improved agreement seen by S17 in the Hertzsprung–Russell diagram suggests the discrepancy is related to the measured masses of the stars. To test this we used the  $K_A$  and  $K_B$  values from *Gaia* to obtain slightly higher masses and a good fit in the mass–radius diagram for an age of  $800 \pm 50$  Myr. However, this results in an increase in the predicted  $T_{\text{eff}}$ s, which must then be brought down by adopting a higher metallicity of at least  $Z = 0.03$ .

HO Tel would benefit from more detailed spectroscopic study. Forthcoming data releases from *Gaia* will contain more epochs of spectroscopy, and the individual RV measurements from the *RVS* spectrometer, so will help in this work. Ground-based spectra would also be useful in determining the  $T_{\text{eff}}$ s and photospheric chemical compositions of the stars to better precision and accuracy.

### Acknowledgements

We thank the anonymous referee for a positive and extraordinarily prompt report. This paper includes data collected by the *TESS* mission and obtained from the MAST data archive at the Space Telescope Science Institute (STScI). Funding for the *TESS* mission is provided by the NASA's Science Mission Directorate. STScI is operated by the Association of Universities for Research in Astronomy, Inc., under NASA contract NAS 5–26555. This work has made use of data from the European Space Agency (ESA) mission *Gaia*<sup>\*</sup>, processed by the *Gaia* Data Processing and Analysis Consortium (DPAC<sup>†</sup>). Funding for the DPAC has been provided by national institutions, in particular the institutions participating in the *Gaia* Multilateral Agreement. The following resources were used in the course of this work: the NASA Astrophysics Data System; the *Simbad* database operated at CDS, Strasbourg, France; and the arXiv scientific paper preprint service operated by Cornell University.

\*<https://www.cosmos.esa.int/gaia>

†<https://www.cosmos.esa.int/web/gaia/dpac/consortium>

## References

- (1) D. Sürgit *et al.*, *New Astronomy*, **54**, 109, 2017.
- (2) J. Andersen, *A&ARv*, **3**, 91, 1991.
- (3) G. Torres, J. Andersen & A. Giménez, *A&ARv*, **18**, 67, 2010.
- (4) E. Lastennet & D. Valls-Gabaud, *A&A*, **396**, 551, 2002.
- (5) C. del Burgo & C. Allende Prieto, *MNRAS*, **479**, 1953, 2018.
- (6) J. Southworth, *The Observatory*, **140**, 247, 2020.
- (7) J. Southworth, *Universe*, **7**, 369, 2021.
- (8) W. Strohmeier, R. Knigge & H. Ott, *IBVS*, **81**, 1, 1965.
- (9) T. A. T. Spoelstra & C. J. van Houten, *A&AS*, **7**, 83, 1972.
- (10) L. A. Crause *et al.*, *Journal of Astronomical Telescopes, Instruments, and Systems*, **5**, 024007, 2019.
- (11) T. Walraven & J. H. Walraven, *BAN*, **15**, 67, 1960.
- (12) G. Pojmański, *A&A*, **47**, 467, 1997.
- (13) E. Hog *et al.*, *A&A*, **355**, L27, 2000.
- (14) Gaia Collaboration, *A&A*, **649**, A1, 2021.
- (15) A. J. Cannon & E. C. Pickering, *Annals of Harvard College Observatory*, **98**, 1, 1923.
- (16) K. G. Stassun *et al.*, *AJ*, **158**, 138, 2019.
- (17) R. M. Cutri *et al.*, *2MASS All Sky Catalogue of Point Sources* (NASA/IPAC Infrared Science Archive, Caltech, US), 2003.
- (18) G. R. Ricker *et al.*, *Journal of Astronomical Telescopes, Instruments, and Systems*, **1**, 014003, 2015.
- (19) Lightkurve Collaboration, 'Lightkurve: Kepler and TESS time series analysis in Python', Astrophysics Source Code Library, 2018.
- (20) J. M. Jenkins *et al.*, in *Proc. SPIE*, 2016, *Society of Photo-Optical Instrumentation Engineers (SPIE) Conference Series*, vol. 9913, p. 99133E.
- (21) J. Southworth, P. F. L. Maxted & B. Smalley, *MNRAS*, **351**, 1277, 2004.
- (22) J. Southworth, *A&A*, **557**, A119, 2013.
- (23) R. F. Sistero & B. A. Candelero, *IBVS*, **1666**, 1, 1979.
- (24) J. Eastman, R. Siverd & B. S. Gaudi, *PASP*, **122**, 935, 2010.
- (25) R. E. Wilson & E. J. Devinney, *ApJ*, **166**, 605, 1971.
- (26) R. E. Wilson, *ApJ*, **234**, 1054, 1979.
- (27) J. Southworth *et al.*, *MNRAS*, **414**, 2413, 2011.
- (28) R. E. Wilson & W. Van Hamme, *Computing Binary Star Observables* (Wilson-Devinney program user guide), available at <ftp://ftp.astro.ufl.edu/pub/wilson>, 2004.
- (29) W. Van Hamme, *AJ*, **106**, 2096, 1993.
- (30) J. Southworth *et al.*, *MNRAS*, **497**, L19, 2020.
- (31) J. Southworth & D. M. Bowman, *MNRAS*, **513**, 3191, 2022.
- (32) J. Southworth & D. M. Bowman, *The Observatory*, **142**, 161, 2022.
- (33) Z. Jennings *et al.*, *MNRAS*, **527**, 4052, 2024.
- (34) A. Prša *et al.*, *ApJS*, **227**, 29, 2016.
- (35) J. Southworth, *The Observatory*, **141**, 234, 2021.
- (36) Gaia Collaboration, *A&A*, **595**, A1, 2016.
- (37) Gaia Collaboration, *A&A*, **674**, A1, 2023.
- (38) Gaia Collaboration, *A&A*, **674**, A34, 2023.
- (39) J. Southworth, *The Observatory*, **143**, 165, 2023.
- (40) D. Bashi *et al.*, *MNRAS*, **517**, 3888, 2022.
- (41) A. Tokovinin, *AJ*, **165**, 220, 2023.
- (42) M. L. Marcussen & S. H. Albrecht, *AJ*, **165**, 266, 2023.
- (43) A. Prša *et al.*, *AJ*, **152**, 41, 2016.
- (44) J. Southworth, P. F. L. Maxted & B. Smalley, *A&A*, **429**, 645, 2005.
- (45) J. Southworth, in *Living Together: Planets, Host Stars and Binaries* (S. M. Rucinski, G. Torres & M. Zejda, eds.), 2015, *Astronomical Society of the Pacific Conference Series*, vol. 496, p. 321.
- (46) P. Kervella *et al.*, *A&A*, **426**, 297, 2004.
- (47) A. Bressan *et al.*, *MNRAS*, **427**, 127, 2012.